

Deep cerebellar neurons mirror the spinal cord's gain to implement an inverse controller

Rodrigo Alvarez-Icaza · Kwabena Boahen

Received: 31 January 2011 / Accepted: 29 June 2011 / Published online: 26 July 2011
© Springer-Verlag 2011

Abstract Smooth and coordinated motion requires precisely timed muscle activation patterns, which due to biophysical limitations, must be predictive and executed in a feed-forward manner. In a previous study, we tested Kawato's original proposition, that the cerebellum implements an inverse controller, by mapping a multizonal microcomplex's (MZMC) biophysics to a joint's inverse transfer function and showing that inferior olivary neuron may use their intrinsic oscillations to mirror a joint's oscillatory dynamics. Here, to continue to validate our mapping, we propose that climbing fiber input into the deep cerebellar nucleus (DCN) triggers rebounds, primed by Purkinje cell inhibition, implementing gain on IO's signal to mirror the spinal cord reflex's gain thereby achieving inverse control. We used biophysical modeling to show that Purkinje cell inhibition and climbing fiber excitation interact in a multiplicative fashion to set DCN's rebound strength; where the former primes the cell for rebound by deactivating its T-type Ca^{2+} channels and the latter triggers the channels by rapidly depolarizing the cell. We combined this result with our control theory mapping to predict how experimentally injecting current into DCN will affect overall motor output performance, and found that injecting current will proportionally scale the output and unmask the joint's natural response as observed by motor output ringing at the joint's natural frequency. Experimental verification of this prediction will lend support to a MZMC as a joint's inverse controller and the role we assigned underlying biophysical principles that enable it.

Keywords Motor cortex · Cerebellum · Spinal cord reflexes

1 Introduction

Smooth and coordinated motion requires precisely timed motor commands to drive our musculoskeletal system, yet despite all evidence suggesting that this is the cerebellum's responsibility, the mechanisms by which it does this remain unknown. Even a simple task like reaching requires precise orchestration of every muscle within your arm, each contributing precisely metered torques around the shoulder, elbow, and wrist that together generate a smooth hand trajectory that stops on target. Muscle's slow and viscoelastic response together with long feedback delay, due to axonal conduction, forbid improvising during motion execution; instead, this precise muscle activation sequence must have been previously rehearsed, and must be executed in a feed-forward fashion. Disturbing the cerebellum makes motion erratic and imprecise (Ghez and Fahn 1985), suggesting that it is its responsibility to properly time motor commands; however, how its biophysics interact to learn and generate these precisely-timed motor commands remains a mystery.

Cerebellar models lack sufficient biophysical detail to explain how the rich cellular dynamics, expressed by all cell types within the olivo–cerebellar complex, generate precisely timed motor commands. The earliest Marr (1969) and Albus (1971) models were mostly inspired by the anatomical connectivity patterns, considering neurons as instantaneous threshold elements that responded to sensory context, such that motions were sequenced by changing sensory input due to the motion itself. Fujita (1982) proposed that Golgi cells delay sensory signals jumping from mossy fibers to parallel fibers, enabling Purkinje cells (PC) to learn spatiotemporal

R. Alvarez-Icaza (✉) · K. Boahen
Department of Bioengineering, Stanford University, Stanford, USA
e-mail: rodrigoa@stanford.edu

K. Boahen
e-mail: boahen@stanford.edu

patterns; this idea was expanded by Barto and colleagues' into the Adjustable Pattern Generator model (Berthier et al. 1993), which incorporates the effects of network dynamics but still fails to account for cellular dynamics. Kawato suggested that motor errors imprint a joint's inverse model onto the cerebellar cortex when he mapped his feedback-error learning paradigm to the cerebellum's architecture (Kawato and Gomi 1992), but neither his model nor his mapping considers cellular dynamics. Only recently did Wetmore et al. (2008) and De Shutter (2009) propose how PC pauses—tuned to the exact dynamics of deep cerebellar nuclear (DCN) cells—trigger rebounds as a cerebellar readout mechanism. Despite a developing trend to include biophysical details, we are still missing an integrated view that accounts for the rich diversity in cellular dynamics present within the cerebellum, without which, it will be impossible to unravel its mysteries and its computational role.

In particular, cerebellar models have traditionally considered DCN as a relay station where PC inhibition modulates the MF pathway, failing to account for the computational role of its rich membrane dynamics. While Marr (1969) simply assumed that PC inhibition would be converted into appropriate elemental movements somewhere in the CNS, for Albus (1971) pauses in PC activity selected elemental commands controlled by DCN; in both cases the role of DCN as the cerebellum's output was not well-developed. Discovering that DCN cells can express powerful Ca^{2+} rebounds from inhibition (Jahnsen 1986; Llinas and Muhlethaler 1988) put into question PC's purely inhibitory role and inspired speculation regarding whether these rebounds could be a mechanism to distinguish between slowly changing inhibition from PC simple spikes and fast transients from PC complex spikes (Aizenman and Linden 1999). Kystler and De Zeeuw (2003) and Kistler et al. (2000) then proposed that delay, introduced by these rebounds, gates reverberating activity around the cerebellar cortico-nuclear loop, but it was only recently that Wetmore et al. (Wetmore et al. (2008)) gave serious attention to DCN's biophysical properties when he proposed that rebound dynamics act as a filter (or lock) to prevent expression of inappropriate motor responses that are stored in cerebellar cortex but do not match the correct temporal pattern. Similarly, Schutter and Steuber (2009) suggest that DCN's dynamics decode pauses in PC's simple spike train, which form a temporal code to trigger rebounds, and whose amplitude is preset by a rate code in the regular simple spiking patterns prior to the pause.

In a previous study we mapped the biophysics of a cerebellar multizonal microcomplex (MZMC) (Apps and Garwicz (2005))—the loop formed by deep cerebellar nucleus, inferior olive (IO), and Purkinje cells—onto an inverse controller and showed how IO's membrane dynamics can mirror the joint's dynamics. To develop intuition, we used control theory to model the biomechanics of a single joint as a harmonic

oscillator and the spinal stretch reflex as a closed loop controller; and to overcome performance limitations of the closed-loop, imposed by physiological signaling delay, we proposed driving it through its inverse transfer function. We found that the architecture and computational roles of this inverse transfer function could be mapped onto the anatomy and electrophysiology of a MZMC, where IO oscillations would mirror the biomechanics' oscillatory nature and DCN, in combination with PC, would implement the spinal cord's gain factor (Fig. 1). As a first step in validating the plausibility of this mapping, we used as a biophysical IO model (Manor et al. (1997); Chorev et al. (2006)) to determine the range of natural frequencies and damping ratios that these cells could express, and found that, indeed, it is comparable to that of the biomechanics (Alvarez and Boahen (Submitted 2011)). Here we expand on our mapping's predictions and show how within the DCN, PC inhibition interacts in a multiplicative fashion with CF excitation, effectively implementing a gain on IO's signal that mirrors the spinal cord's loop gain.

2 Methods

2.1 Biomechanical modeling

We had previously modeled a biomechanical joint as a harmonic oscillator and the spinal cord's stretch reflex as a PD closed-loop controller, and mapped this system's inverse model onto a microzone's biophysics (Alvarez and Boahen Submitted 2011). We modeled the joint's biomechanics as a mass connected to a spring, a damper and a force producing element and described by $M\ddot{x} + \beta\dot{x} + Kx = F(t)$; where K and β represent the muscles' elasticity and viscosity respectively, M represents the mass, x is M 's displacement and $F(t)$ represents the net force produced by the antagonistic muscle pair acting around the joint. We then modeled the spinal cord's stretch reflex as a closed-loop PD controller around the joint's biomechanics ($P(s)$), with proportional (K_P) and derivative (K_D) gains such that $J(s) = (K_P + K_D \cdot s) \cdot P(s) / [1 + (K_P + K_D \cdot s) \cdot P(s)]$; and, to improve overall system performance beyond the limits of the closed-loop, we drove this controller—in feed forward fashion—through an inverted copy of itself. Finally, we mapped this inverse controller ($1/J(s)$) to a cerebellar MZMC's architecture, which predicted that descending commands are looped around the MZMC within which IO mirrors the joint's oscillatory dynamics and PC and DCN mirror the spinal cord's loop gain (Fig. 1).

2.2 DCN biophysical modeling

We modeled DCN cells biophysically to test if their rebounds can implement a gain factor on IO's signal, as predicted by

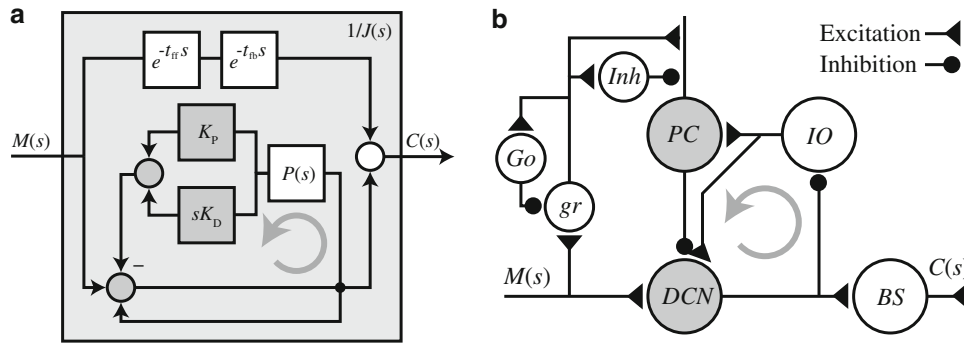


Fig. 1 **a** Multizonal microcomplex maps to an inverse controller: a Block diagram for a joint’s inverse transfer function’s $1/J(s)$ implementation illustrating a top path that mirrors the spinal reflex’s total delay and a bottom path that mirrors the spinal cord’s and the musculoskeleton’s dynamics. **b** Cerebellar microzone diagram, illustrating

an analogous loop around a microzone that hypothetically computes $1/J(s)$. *DCN* deep cerebellar nucleus, *BS* brainstem, *IO* inferior olive, *PC* Purkinje cells, *Go* golgi cells, *gr* granule cells, and *Inh* inhibitory interneurons. Adapted from Submitted 2011

our MZMC mapping. Following Wetmore’s (Wetmore et al. (2008)) footsteps, we focused on the role of dendritic Ca^{2+} channels on rebound generation and thus implemented a single-compartment, conductance-based model with a T-type Ca^{2+} conductance, a high-voltage-activated (HVA) Ca^{2+} conductance, a generic leak conductance, and excitatory and inhibitory synaptic conductances. Specifically,

$$C_m \cdot dV/dt = g_T \cdot n \cdot l \cdot (V_{Ca} - V) + g_{HVA} \cdot o^2 \cdot p \cdot (V_{Ca} - V) + g_L \cdot (V_L - V) + g_{PC} \cdot (V_{GABA} - V) + g_{CF} \cdot (V_{Glu} - V) + I_{in}$$

describes the cell’s dynamics; where V represents the cell’s membrane potential and C_m the cell’s capacitance; g_T , g_{HVA} , g_L , g_{PC} , and g_{CF} , respectively, represent the maximum conductances for T-type, HVA, leak, PC inhibition, and CF excitation; I_{in} represents a generic input current; V_{Ca} , V_L , V_{GABA} , and V_{Glu} represent reversal potentials for the Ca^{2+} , leak, inhibitory, and excitatory conductances; and n , l , o , and p represent activation and inactivation variables for both Ca^{2+} channel species (Fig. 2). The T-type and HVA channels dynamics were identical to Wetmore et al. (2008) and Mainen (1996), respectively, (see appendix for the equations and constants) and the leak conductance and reversal potential was set such that the cell exhibited a 12 min time constant and a -58 mV resting potential (Llinas and Muhlenthaler 1988). Like Wetmore, we explored a wide range of g_T values (from 0.3 to 0.6 ms/cm^2), but unlike them we used smaller g_{HVA} values to insure that cells expressed graded Ca^{2+} rebounds and not Ca^{2+} spikes (see Sect. 4); in particular we choose $g_T = 0.45$ ms/cm^2 and $g_{HVA} = 0.045$ ms/cm^2 for our single cell simulations.

We modeled how inhibition primes DCN cells for rebound by deinactivating Ca^{2+} channels. By simplifying the effect of PC simple spikes into a tonic inhibitory current, as opposed to a complex time-varying synaptic conductance dependent

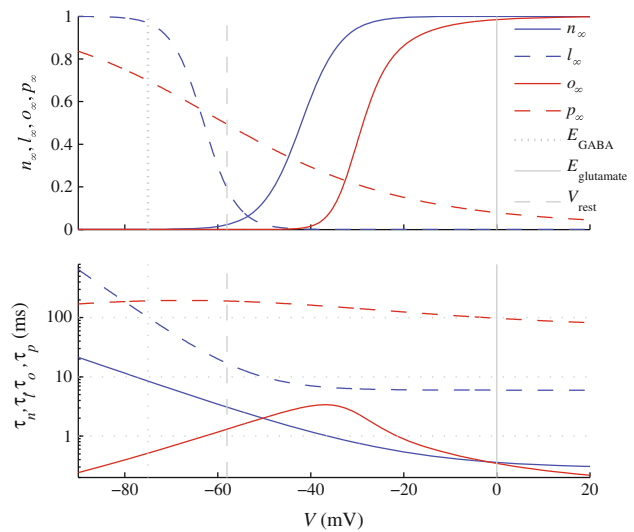


Fig. 2 DCN’s channel dynamics: T-type Ca^{2+} channel activation (n) and inactivation (l) and high-voltage-activated Ca^{2+} channel activation (o) and inactivation (p)

on spike rate, we were able to solve the model’s governing equations (using Matlab’s `fzero` function) and determine the cell’s equilibrium point as a function of inhibitory input current (Fig. 3). Each equilibrium point—the point defined by the steady state values for the membrane potential as well as for the activation and inactivation of T-type and HVA Ca^{2+} channels—defined the cell’s primed state and served as the model’s initial conditions from where we studied rebounds triggered by CF excitation.

Through transient analysis we characterized how a DCN’s primed state determines the strength of its rebound when the cell is released from inhibition. Using Euler’s method—with a time step of $100 \mu s$ —to integrate the model’s differential equations, we primed DCN cells by injecting a long inhibitory current pulse, representing PC simple spikes, and observed the resulting rebound. To quantify the rebound’s

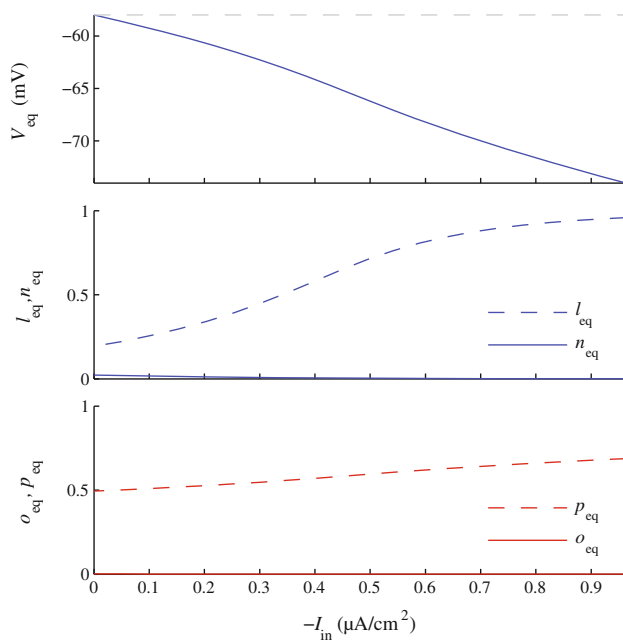


Fig. 3 Priming DCN for rebound: DCN's equilibrium point as a function of PC inhibition, modeled as a tonic inhibitory current injection (higher current corresponds to higher PC simple spiking rate). l_{eq} : T-type Ca^{2+} channel deinactivation; p_{eq} : High-voltage-activated Ca^{2+} channel deinactivation; n_{eq} : T-type Ca^{2+} channel activation; o_{eq} : High-voltage-activated Ca^{2+} channel activation

strength, we measured its peak and computed its overall area (for $V > V_{rest}$). Furthermore, we determined the independent current contributions of T-type and HVA Ca^{2+} channels, which revealed that T-type Ca^{2+} channels govern subthreshold Ca^{2+} rebounds while HVA channel activation results in Ca^{2+} spikes (Fig. 4). Based on this, we constrained DCN priming to that induced by inhibitory currents smaller than $0.4 \mu\text{A}/\text{cm}^2$, as this range results in graded rebound responses.

Through further transient analysis we characterized how CF excitation triggers rebounds and determines their strength (while maintaining inhibition constant). We repeated the previous transient analysis, but this time we used inhibitory and excitatory conductances, instead of tonic currents, to insure that inhibitory and excitatory drive scaled properly as the cell depolarized throughout the rebound. We modeled PC inhibition as a constant GABAergic conductance (g_{PC}), with a -75 mV reversal potential (Hille 2001), and choose its values so that it matched the previously used currents and resulted in identical equilibrium points as before. We modeled CF excitation as a 5 ms pulse on a glutamatergic conductance (g_{CF}), with a 0 mV reversal potential (Chun et al. 2003). We quantified the rebound's strength by measuring its peak and computing its overall area as before.

We quantified how PC inhibition modulates the rebound's sensitivity, as measured by the slope of the rebound's peak and area, to CF excitation. We primed DCN cells using a

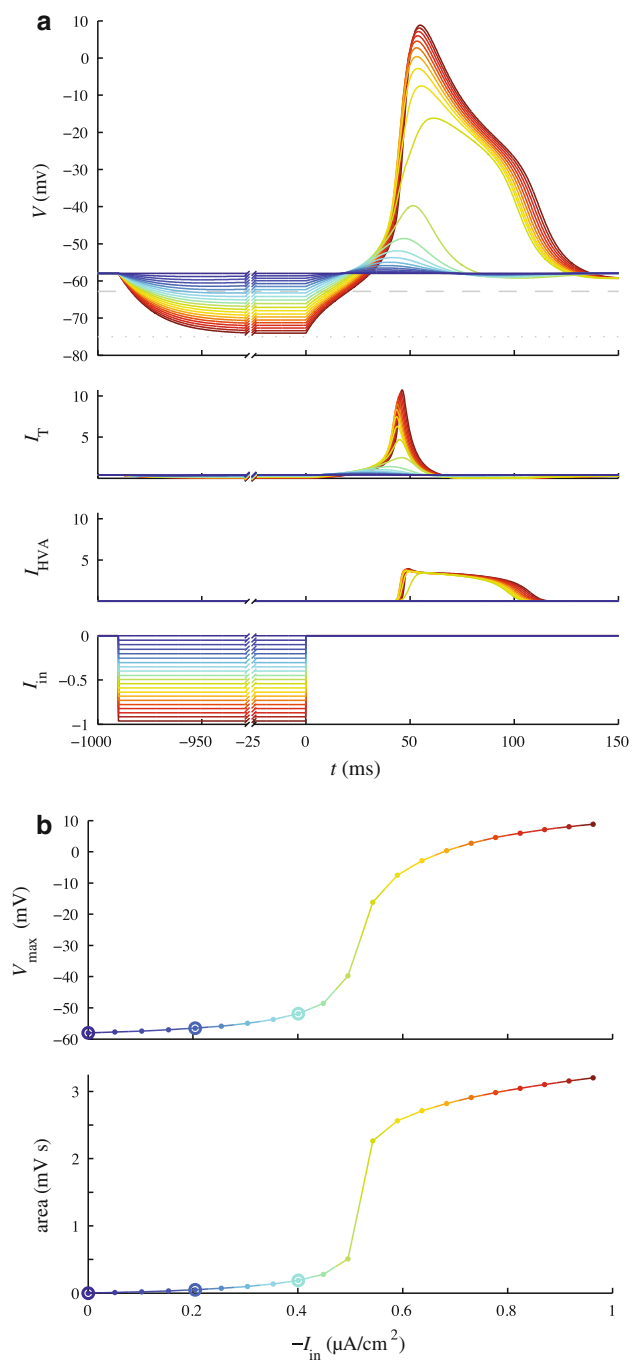


Fig. 4 DCN's free rebounds: DCN rebounds when released from an inhibitory current injection. Warm colors indicate stronger inhibition. **a** Membrane voltage, T-type Ca^{2+} current, high-voltage-activated (HVA) Ca^{2+} current, and inhibitory input current (I_{in}). All currents are in $\mu\text{A}/\text{cm}^2$. **b** Rebound peak (V_{max}) and rebound area as a function of inhibitory current magnitude

g_{PC} range that would not trigger Ca^{2+} spikes on its own (0 – $0.3 \text{ mS}/\text{cm}^2$), and for each g_{PC} value we ran multiple trials where we varied g_{CF} pulse's strength (from 0 to $0.1 \text{ mS}/\text{cm}^2$ for 5 ms) and measured the rebound's peak and area. For each g_{PC} value, we fit a linear model to the rebound's peak and

area, and used the slope to measure the rebound’s sensitivity to g_{CF} . To perform these fits, we choose the widest overall range where the rebound is most sensitive to g_{CF} (0.038–0.059 mS/cm² for a single cell and 0.038–0.083 mS/cm² for the heterogeneous population) and the fit still returned an $R^2 > 0.85$. The resulting slopes, one for each g_{PC} value, tell us how PC inhibition modulates the rebound’s sensitivity to CF input (Figs. 5 and 6).

To determine if PC inhibition can robustly modulate the rebound’s sensitivity to CF excitation, we modeled a heterogeneous DCN cell population. We repeated the previous simulations across cells with various combinations of g_T (0.3–0.6 mS/cm²) and g_{HVA} (0.01–0.08 mS/cm²) and averaged each trial’s resulting membrane potential waveforms across the cell population. From the averaged membrane potentials we measured the rebound’s peak and area and used these, as before, to compute the rebound’s sensitivity to CF excitation and how it is modulated by PC inhibition (Fig. 6).

2.3 Implications for biomechanical control

To make experimentally testable predictions, we quantified how current injection affects the rebound’s sensitivity to CF excitation. Once again, we repeated the previous transient simulations and analysis, but this time we added an experimental current injection (I_{in}) (−0.3–0.3 μA/cm²) to our stimulation protocol. Comparing the results to the case without I_{in} reveals how a tonic input current adds to PC’s effect and biases the rebound’s sensitivity to CF excitation (Fig. 7).

Using our control theory model, we characterized how experimentally manipulating the rebound’s sensitivity to CF excitation would affect motor output by simulating a mismatch between the inverse transfer function’s gains (K_{PPC} and K_{DPC}) and the spinal cord’s loop gains (K_P and K_D). As in our previous study (Alvarez and Boahen Submitted 2011), we use Matlab’s Control System Toolbox to implement an exemplary elbow joint described by $T(s) = 1/J'(s) \cdot J(s)$ and simulated its transient and frequency response using Matlab’s built-in functions lsim() and bode(), respectively. We drove $T(s)$ with a sigmoid, described by $m(t) = 1/(1 + \exp(-(t - t_0)/\tau))$ where $\tau = 15$ ms and $t_0 = 100$ ms, and measured the motor output’s maximum percent overshoot, its rise-time (from 10 to 90%), and its settling time (to within a ± 5% error band) as a function of mismatch between K_{PPC} and K_P and between K_{DPC} and K_D (Fig. 8); we varied K_{PPC} and K_{DPC} in the same proportion.

3 Results

Our mapping predicts that a MZMC loop’s gain must mirror the spinal cord’s gain, and therefore there must be a multiplicative interaction between PC inhibition and CF excitation

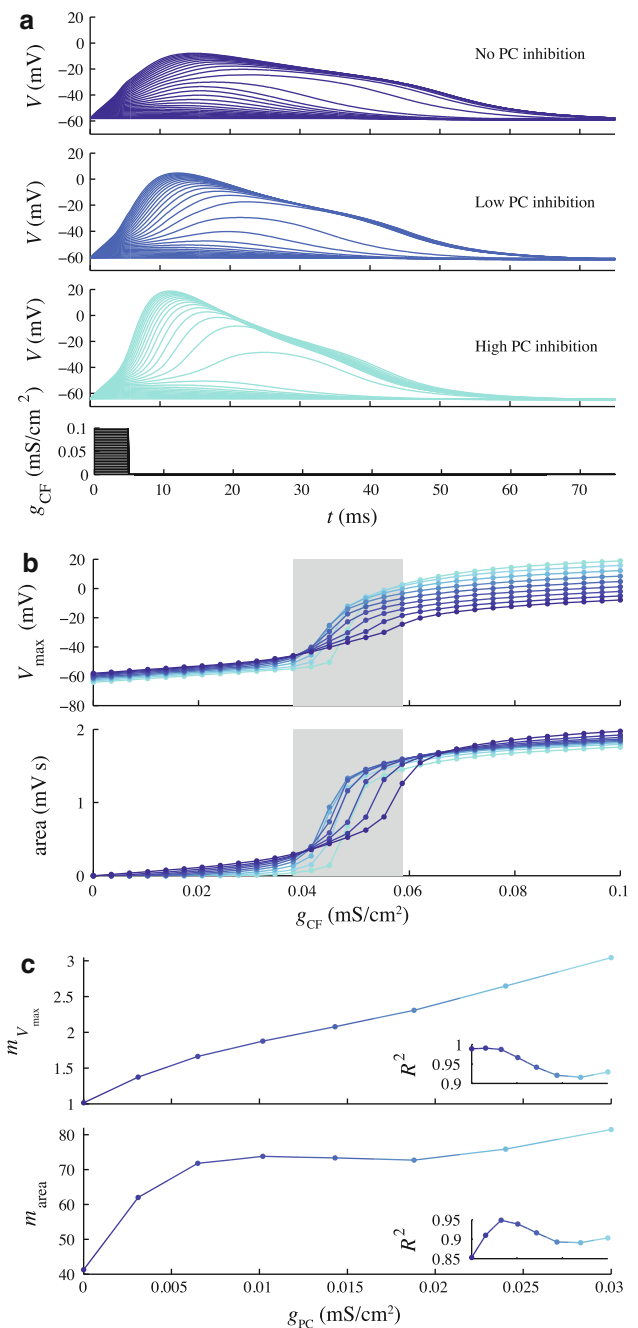


Fig. 5 Climbing fiber-triggered rebounds: DCN rebounds primed by PC inhibition and triggered by climbing fiber excitation (CF), the latter modeled as 5 ms steps in glutamatergic conductance (g_{CF}). **a** Rebounds when primed with no inhibition ($g_{PC} = 0.0$ mS/cm²), low PC inhibition ($g_{PC} = 0.014$ mS/cm²) and high PC inhibition ($g_{PC} = 0.037$ mS/cm²); these samples correspond to encircled points in Fig. 4b: Rebound peak (V_{max}) and rebound area as a function of CF excitation (horizontal axis) and PC priming (colored lines consistent with Fig. 4). **c** Slope from linear fit to V_{max} and area data within grayed region in (b), slopes are in units of mV/mS/cm² and mVs/mS/cm², respectively. Inset illustrates goodness of fit

at the DCN. In our control theory model, a gain factor must be applied to the oscillator’s output within the joint’s inverse transfer function. Due to its rich Ca²⁺ dynamics, we propose

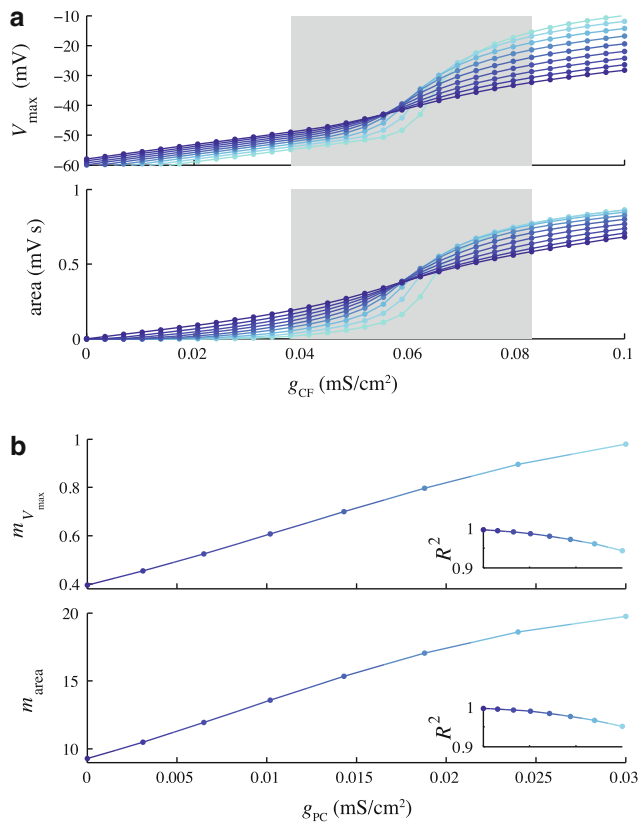


Fig. 6 Gain implementation by a DCN population: rebounds primed by PC inhibition and triggered by CF excitation (as in Fig. 5) for a heterogeneous DCN population expressing a maximum T-type Ca²⁺ conductance (g_T) range from 0.3 to 0.6 mS/cm², and a maximum HVA Ca²⁺ conductance (g_{HVA}) within the range $g_T/10 \pm 0.020$ mS/cm². **a** Rebound peak (V_{\max}) and rebound area as a function of CF excitation (horizontal axis) and PC priming (colored lines consistent with Figs. 4 and 5). **b** Slope from linear fit to V_{\max} and area data within grayed region in (a), slopes are in units of mV/mS/cm² and mVs/mS/cm², respectively. *Inset* illustrates goodness of fit

that DCN implements this gain factor, set by Purkinje cell inhibition, on IO's signal.

Using a biophysical DCN model we determined how hyperpolarization, due to PC inhibition, primes the cell for rebound by deactivating T-type Ca²⁺ channels such that subsequent depolarization, due to CF excitation, triggers a rebound. Specifically, through transient analysis of a single-compartment cell we characterized how interactions between these two inputs determine the rebound's strength, and found that within the range where PC inhibition and CF excitation are strong enough to activate T-type Ca²⁺ channels—but not too strong to activate the cell's HVA Ca²⁺ channels—we observe graded rebound strengths that encoded the product of the two inputs; beyond this range, activation of HVA Ca²⁺ channels results in a stereotypical all-or-none Ca²⁺ spike which is thought to rarely be expressed in vivo (Alvina et al. 2008). Furthermore, we found this to be true for cells expressing the entire physiologically realistic g_T range

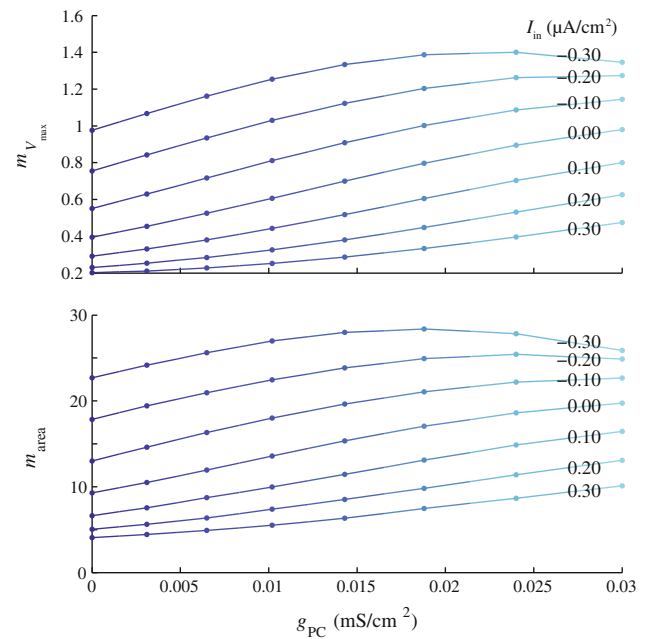


Fig. 7 Effects of current injection on DCN's gain factor: DCN's gain factor resulting from experimental current injection (I_{in}), as measured by slope from linear fits within same population as in Fig. 6. Slopes are in units of mV/mS/cm² and mVs/mS/cm², respectively. *Inset* illustrates goodness of fit

(0.3 to 0.6 mS/cm²), as long their g_{HVA} expression was not too large ($g_{HVA} < g_T/10 + 0.02$ mS/cm²) to significantly reduce the threshold for all-or-none Ca²⁺ spikes.

3.1 Gain modulation in a biophysical DCN model

PC inhibition deinactivates both T-type and HVA Ca²⁺ channels, but it is T-type Ca²⁺ channels that prime DCN cells for rebound. Increasing PC simple spiking above the baseline rate of 40 Hz (Berthier and Moore 1986) hyperpolarizes DCN's cells, via a GABAergic synaptic conductance with a -75 mV reversal potential, below DCN's natural resting potential of -58 mV (Llinas and Muhlethaler 1988). Within this viable hyperpolarization range, from -58 to -75 mV, the T-type Ca²⁺ channels undergo a large change in inactivation—from 0.2 to 0.98—with a relatively fast time-constant (20–100 ms). In contrast, the HVA Ca²⁺ channels undergo a smaller change in inactivation—from 0.5 to 0.7—with a slower time constant (180 ms) (Figs. 2 and 3). T-type Ca²⁺ channel deinactivation thus stores a reliable history of the cell's hyperpolarization state, so that when the cell is depolarized, it will be the T-type Ca²⁺ channel deinactivation that shapes the initial Ca²⁺ rebound.

While T-type Ca²⁺ channel activation governs graded Ca²⁺ rebounds from inhibition, HVA channel activation produces all-or-none Ca²⁺ spikes. When a primed DCN cell is depolarized—by releasing the cell from inhibition or by

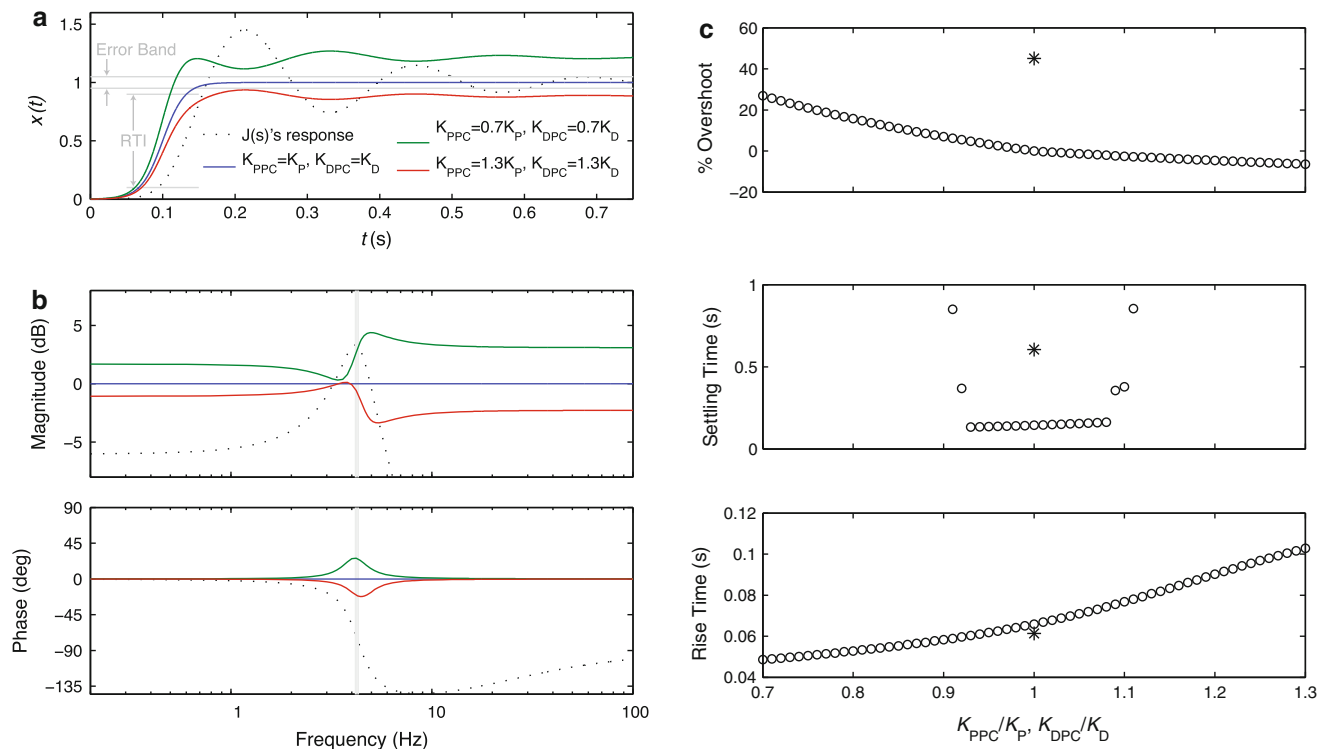


Fig. 8 Disturbing DCN: experimental predictions: **a** $T(s)$'s temporal response to a smoothed input step when mismatch between DNC's gain factor and the spinal cord's loop gain factor is experimentally induced. *RTI* range over which rise time is computed. **b** $T(s)$'s frequency

response for same cases as in a, illustrating the unmasking of the joint's natural response. **c** Output's percent overshoot, settling time and rise time as a function of gain mismatch; all metrics are computed relative to the ideal response

direct excitation—T-type Ca^{2+} channels are the first to activate, around -60 mV. This activation combines with the primed deinactivation and sets a Ca^{2+} current that continues to depolarize the cell until these channels inactivate again. If the T-type Ca^{2+} channel current (or depolarizing excitation) is not strong enough to depolarize the cell beyond -38 mV, then HVA channels are not activated and the rebound decays rapidly (Fig. 4 blue through cyan); however, if the current is strong enough to depolarize the cell beyond -38 mV, then HVA channels are activated and their Ca^{2+} current will continue depolarizing the cell. Owing to HVA channel's slow inactivation time constant (about 100 ms), activating these channels will hold the cell in a depolarized state for about 65 ms, resulting in a more stereotyped all-or-none Ca^{2+} spike (Fig. 4 aqua through red traces).

Therefore, to trigger a graded response, excitation from CF collaterals must depolarize the cell enough to activate T-type Ca^{2+} channels, but without crossing the threshold for triggering a HVA Ca^{2+} spike. While keeping PC inhibition constant, we varied the strength of CF excitation and found a sweet spot over which CF excitatory drive is strong enough to activate T-type Ca^{2+} channels, but not too strong to activate HVA channels. Within this range, the rebound's peak and its area are most sensitive to CF excitation; below this

range the rebound's peak and area are not very sensitive to CF strength, and above this range the response saturates as the cell fires a Ca^{2+} spike (Fig. 5).

Within the range where CF excitation activates T-type Ca^{2+} channels, but not HVA channels, priming by PC inhibition and triggering by CF excitation interact in a multiplicative fashion. The sensitivity of the rebound's peak and area to CF excitation increases with PC inhibition. However, for the rebound's area the sensitivity increases much more rapidly, and therefore the rebound's response quickly saturates, appearing as if PC inhibition decreases the threshold for a Ca^{2+} spike. Whether the downstream readout for a single cell is the rebound's peak or area, priming the cell through PC inhibition strengthens the cell's response to CF excitation (Fig. 5).

A heterogeneous population of DCN cells exhibits this multiplicative interaction over a wider range than any single cell. Averaging voltage waveforms from DCN cells expressing variable T-type and HVA maximum conductances expands the range over which rebound metrics are most sensitive to CF excitation; and unlike the results for a single cell where only the rebound's peak follows a linear trend, for a DCN cell population the rebound's area also grows linearly with CF excitation (Fig. 6). On one hand, these results

are consistent through the entire physiologically realistic g_T range (from 0.3 to 0.6 mS/cm²); below this range DCN cells do not express Ca²⁺ rebounds and above this range they become spontaneous oscillators. On the other hand, although a wide g_{HVA} range (0.025–0.065 mS/cm²) still shows a linear trend for the rebound's peak, linearity improves when the g_{HVA} range is constrained around $g_T/10 \pm 0.020$ mS/cm²; actually, increasing the g_{HVA} range around $g_T/10$ improves linearity at the expense of reducing the rebound's sensitivity to g_{CF} (not shown). Overall, by expanding the range of this effect and improving its linearity, channel expression heterogeneity improves DCN's capacity to implement a multiplicative interaction between PC inhibition and CF excitation (Fig. 6).

3.2 Experimental predictions and biomechanical implications

Experimentally injecting an inhibitory current into DCN adds to PC's priming effect and increases the population's overall gain factor. This inhibitory current adds to PC's GABAergic current to further hyperpolarize the cell, increasing T-type Ca²⁺ channel deactivation, and thus increases the sensitivity of a rebound's peak and area to CF excitation. Inhibitory currents, similar in magnitude to PC's inhibition (0–0.3 μ A/cm²), may therefore increase the population's overall gain factor to approximately 1.75 times its original value. By the same token, excitatory currents of the same magnitudes (0–0.3 μ A/cm²), which depolarize the cell and thus reduce T-type Ca²⁺ channel deactivation, may therefore decrease the population's overall gain factor to approximately 0.33 times its original value (Fig. 7). As a result, we may test our model by dramatically perturbing DCN's gain in vivo through current injection, while observing how this affects overall motor output.

Our control theory model predicts that experimentally introducing mismatch between the DCN's gain and the spinal cord's will scale the overall motor output response and introduce ringing at the biomechanical joint's natural frequency, unmasking the joint's ($J(s)$) natural response. This is easily observed in transient analysis, where the steady state value scales with DCN gain and the waveform's peaks and troughs line up—albeit phase shifted for reduced gain—with $J(s)$'s natural response, as well as in the frequency response, where there is a boost around the biomechanical joint's natural frequency (Fig. 8). Analytically, $J(s)$'s poles define the whole system's ($T(s)$) poles and thus, when not properly canceled (because of mismatch), these poles emerge and dominate the system's output, setting its resonance frequency at the biomechanical joint's natural frequency. Although mismatch between DCN's gain and the spinal loop's gain has a strong effect on steady state value, percent overshoot, settling time,

and rise time, remarkably, motor output always rings at the biomechanic's natural frequency.

4 Discussion

We presented results from a biophysical model showing how PC inhibition primes the DCN for rebound, modulating the effects of CF excitation in a multiplicative fashion thus validating that PC and the DCN implement gain on IO's signal—a prediction of our MZMC mapping. Sustained hyperpolarization by PC inhibition deinactivates the cell's T-type Ca²⁺ channels—priming the cell—so that an abrupt depolarization by CF excitation may trigger a depolarizing Ca²⁺ current whose magnitude is the product of the channel's inactivation and activation. Through transient analysis we extended this intuition and verified that there is a wide range over which priming and triggering are strong enough to activate the DCN's T-type Ca²⁺ channels—but not HVA Ca²⁺ channels—and thus produce rebounds whose strength, as measured by the rebound's peak and area, is set by the product of PC inhibition and CF excitation. Below this range, T-type Ca²⁺ channels are not activated and thus PC inhibition does not increase the rebound's sensitivity to CF excitation, and above this range HVA Ca²⁺ channels are activated and DCN fires an all-or-none Ca²⁺ spike (Figs. 5 and 6). Altogether, it is clear that PC inhibition can modulate the sensitivity of DCN rebounds to CF excitation in a multiplicative fashion.

Our choice to focus on graded rebounds as DCN's readout mechanism is justified by there being little direct evidence supporting the prevalence of Ca²⁺ spikes in vivo. Our modeling results showed two distinct rebound regimes which could be induced in any given cell expressing some combination of T-type and HVA channels: one where T-type Ca²⁺ currents induced rebounds with graded amplitude and another where HVA Ca²⁺ currents induced in an all-or-none stereotypical Ca²⁺ spike (Fig. 4); the latter could always be induced if the cell was sufficiently primed or depolarized, and as expected, higher HVA Ca²⁺ expression lowered the threshold for Ca²⁺ spikes. Given that in our MZMC mapping DCN must output an analog signal, we constrained our model to express a weaker HVA Ca²⁺ conductance (around $g_T/10$), as compared to that used by Wetmore et al. (2008), and only studied stimuli that resulted in graded rebounds (Figs. 5 and 6). Although the earliest physiological recordings clearly showed that in vitro DCN cells express strong Ca²⁺ spikes (Jahnsen 1986; Llinas and Muhlethaler 1988; Aizenman and Linden 1999), our choice to focus on graded rebounds is justified by evidence showing a very low prevalence for Ca²⁺ spikes in vivo (Alvina et al. 2008).

Our MZMC mapping assumes that direct excitation from climbing fiber collaterals into DCN must trigger rebounds, rather than PC disinhibition, which is plausible but has not been definitely shown experimentally. Anatomically, of their total synaptic input, DCN cells receive about 5% from the IO, about 10–35% from mossy fibers and the remaining 60–85% from PCs (Chan-Palay 1973), so IO accounts for 1/3rd to 1/8th of the total excitatory input. However, physiologically, the earliest DCN recordings revealed the occurrence of short-latency excitatory-post-synaptic-potentials (EPSP) as a result of harmaline injection into the IO (Llinas and Muhlethaler 1988). Furthermore, IO's ability to directly excite DCN has been confirmed by experiments involving direct electrical excitation of the IO (Rowland and Jaeger 2008); however, the complexity of the olivo-nuclear connection, which has an additional indirect pathway through PC inhibition, have made it difficult to rule out the contribution of PC's disinhibition casting doubts on the overall effect that IO has on DCN (Baumel et al. 2009).

Our results, or more precisely our focus on the rebound's peak and area, raise the question of how rebound strength is read out from DCN. We chose to limit our model's complexity to the minimum required for validating a multiplicative interaction between PC and CF pathways, and as such focused on a single compartment—representing DCN's dendrites—expressing well-characterized Ca^{2+} conductances. By ignoring Na^+ spikes we were forced to assume that increases in dendritic potential above the cell's resting potential would appear as a current injection into the soma and thus directly increase the cell's spiking rate above its 25 Hz baseline (Aksenov et al. 2005; Jahnsen 1986; Raman et al. 2000). Based on these assumptions we gauged rebound strength from both the rebound's peak, as a measure of maximum dendritic current injection into the soma, and the rebound's area, as a combined measure of current amplitude and duration.

Our model assumes that joint dynamics, represented within a MZMC, get converted into muscle activation commands, which are in turn distributed to the appropriate flexor or extensor muscles (or their subunits) by neuronal circuits outside of the olivo-cerebellar complex. Our model assumes that a conversion from a position command to a muscle activation command occurs within the spinal cord's servo loop. Furthermore, within our model a joint has a single control input whereas biomechanical joints are driven by multiple agonist and antagonist muscles, some of which may act across more than one joint, therefore requiring carefully distributing any descending command. In our mapping we assume this distribution is handled by either brain stem nuclei that relay cerebellar commands or by the spinal cord's circuitry.

The multiplicative interaction between PC inhibition and CF excitation can be tested experimentally using standard electrophysiological techniques with acutely prepared DCN

slices. For simplicity we stimulated our model by tonically setting the cell's synaptic conductances and our stimulation protocol may be repeated in vitro using a dynamic clamp. The DCN slice preparation will afford the ability to use Na^+ spiking as an additional measure of rebound strength and verify if indeed there is a multiplicative interaction between the two pathways.

Although the gain of spinal reflexes is known, we would need a full MZMC model to establish a quantitative comparison between the spinal cord's gain and the MZMC's gain. Data for spinal cord reflexes (Allum and Mauritz 1984; Bennett 1994) allows us to compute closed-loop gain factors for our control theory model ($K_P = 1$, $K_D = 0.0076$), and we have shown that there is a multiplicative interaction between PC inhibition and CF excitation expressed in DCN's rebound strength. However, the absolute loop gain of the MZMC will also depend on the synaptic mechanisms by which DCN output affects the IO itself (as well as other brain targets). Therefore, we cannot determine the MZMC's loop gain without having a spiking model that closes the loop around IO and DCN.

At the system level, our results predict how experimentally injecting current into DCN will affect its gain factor, and how this in turn, will scale overall motor output and unmask the joint's natural dynamics as seen by output ringing. Through the biophysical DCN model we found that inhibitory current injection adds to PC's priming effect and increase the cell's sensitivity to CF excitation, effectively increasing DCN's gain factor (Fig. 7). Furthermore, using our control theory model we found that increasing the inverse transfer function's gain—which maps to DCN's gain—will increase the outputs steady state value and introduce motor output ringing, at the biomechanical joint's natural frequency. Our model also predicts that inhibitory current injections will advance the outputs phase and reduce the output's rise-time, speeding up the system's response at the expense of ringing; in contrast excitatory current injection will decrease the gain, reducing the outputs steady state and slowing down the system (Fig. 8).

Although we did not model a detailed synaptic stimulation sequence, we modeled the worse case scenario, where PC inhibition remains constant even when CF excitation triggers a complex spike. To minimize the parameter space we reduced synaptic input to one GABAergic and one glutamatergic conductance and set their values such that their effects were within the physiologically observed ranges, instead of implementing detailed GABAergic and glutamatergic synaptic dynamics, each with its own time course, synaptic number, spiking rate, and distribution. Furthermore, to approximate the EPSP physiologically observed from CF excitation (Llinas and Muhlethaler 1988), we activated the glutamatergic conductance for 5 ms; but to avoid speculating about the length, magnitude and even the sign required to properly implement the effects of a PC complex spike—

inevitably triggered by the CF—we assumed the simplest scenario and maintained our GABAergic conductance constant throughout each trial. Most likely, DCN cells actually see a complex spike as a 10 ms pause in PC inhibition (due to the fast spikelets getting lost at the PC axon (Monsivais et al. 2005; Gauck and Jaeger 2000)). Therefore, by ignoring desinhibition subsequent to a complex spike, CF excitation undertakes the full responsibility of rebound initiation.

Dissecting the mechanistic nature of DCN rebounds suggest that the roles played by the PC pathway, the CF pathway and the MF pathways during the slow priming phase, the fast triggering phase and the rebound's expression, respectively, are consistent with our MZMC mapping. Priming is a slow process, due to T-type Ca^{2+} channel's slow inactivation time constant (20–40 ms), which must be dominated by long-standing inhibitory input from PC activity to hold the cell at a hyperpolarized level, and which will set DCN's gain factor. The rebound's trigger must be an abrupt depolarization event, due to T-type Ca^{2+} channel's inactivation speeding up above -58 mV (6–15 ms), for which synchronous excitation from the CF (on a millisecond time scale (Llinas et al. 2004)), which has been shown to carry IO's phase (Mathy et al. 2009), is the ideal candidate and consistent with our mapping. Finally, if MF activity coincides with CF excitation it will further activate T-type Ca^{2+} channels and multiplicatively interact with PC inhibition; otherwise, as long as MF activity is not synchronous and strong enough to trigger a rebound, then it will only act as tonic excitation.

Our mapping predicts that PC's simple spiking rate must prime DCN prior to motion initiation, setting its gain factor, and adapt during motion execution, tracking the joint's effective gain, which is consistent with physiological recordings. Prior to motion initiation, DCN cells must be hyperpolarized by PC inhibition for approximately 20–100 ms to deactivate T-type Ca^{2+} channels thus setting the rebound's strength. Throughout motion execution, DCN cells within the population must continually be primed for rebound and therefore PC inhibition must ensue and their simple spiking rate must track the joint's effective gain. Consistent with our mapping, PC firing patterns during reaching show increased activity approximately 100 ms prior to motion initiation (Fortier et al. 1989; Fu et al. 1997), suitable for priming DCN cells and setting the gain factor, followed by a relatively constant firing rate throughout a reaching motion.

In contrast with the prevailing views that desinhibition triggers DCN rebounds, and that these serve timing purposes (Kistler and Zeeuw 2003; Wetmore et al. 2008; Schutter and Steuber 2009), our mapping and results suggest that it is CF excitation that triggers them, and that their role is scaling IO's signal, not timing the MF or PC pathways. Understandably, the long delay between desinhibition and rebound expression (Llinas and Muhlethaler 1988; Aizenman and Linden 1999) inspired Kistler's model and supports Wetmore's lock-

and-key hypothesis, and may serve a purpose for classical conditioning-like task. However, it is counter intuitive that for motor control tasks, the cerebellum's output stage would introduce the long delay required for priming plus the delay required to passively express the rebound into the motor response, where a short reaction time is a clear evolutionary advantage. Similar to De Schutter and Steuber's proposal our results suggest that ongoing PC simple spiking activity sets the rebounds strength, which can either be precisely adjusted during a planning phase to optimize motion if time allows, but can also have a default value that supports a quick reaction time if required; but unlike in their model, where rebounds are passively triggered by pauses in PC simple spiking trains, in our model direct excitation from CF collaterals expedites rebounds, dramatically reducing their onset to a few milliseconds (Fig. 5).

In combination with our previous work showing that IO is capable of mirroring the biomechanic's dynamics, by now showing that DCN is capable of implementing a gain factor on IO's signal to mirror the gain of the spinal cord's loop, we have completed a preliminary validation, at the biophysical level, of our mapping between a MZMC and a joint's inverse transfer function thus supporting the hypothesis of the cerebellum as an inverse controller. We proposed that a MZMC acts as an analog computer that implements a joint's inverse transfer function, and we have now shown that the IO and the DCN support the two key computational primitives required: an oscillator and a multiplier, respectively. This framework has already offered experimentally testable predictions that link the cerebellum's biophysics to their computational abstraction and to overall motor performance, but beyond this, the proposed framework will serve as a test bed to explore how ascending feedback from the spinal cord drives cerebellar plasticity to acquire an accurate inverse transfer function by tuning IO's oscillatory dynamics and DCN's effective loop gain. Finally, this framework can be extended to control multiple joints, and in the process explore which anatomical and biophysical properties enable coordination between various MZMCs.

Appendix

T-type Ca^{2+} channel activation

$$dn/dt = (n_{\infty} - n)/\tau_n$$

$$n_{\infty} = (1 + \exp[-(V + 42.0)/4.25])^{-1}$$

$$\tau_n = 0.287 + 0.0711 \cdot \exp(-V/15.8)$$

T-type Ca^{2+} channel inactivation

$$dl/dt = (l_{\infty} - l)/\tau_l$$

$$l_{\infty} = (1 + \exp [(V + 63.0) / 3.50]) - 1$$

$$\tau_l = 5.960 + 0.00677 \cdot \exp (-V / 7.85)$$

HVA Ca^{2+} channel activation

$$o_{\infty} = \alpha_o / (\alpha_o + \beta_o)$$

$$\tau_o = 1 / (2.3 \cdot (\alpha_o + \beta_o))$$

$$\alpha_o = 0.055 \cdot (V + 27) / (1 - \exp (-[V + 27] / 3.8))$$

$$\beta_o = 0.94 \cdot \exp (-[V + 75] / 17)$$

HVA Ca^{2+} channel inactivation

$$p_{\infty} = \alpha_p / (\alpha_p + \beta_p)$$

$$\tau_p = 1 / (2.3 \cdot (\alpha_p + \beta_p))$$

$$\alpha_p = 4.57e - 4 \cdot \exp (-[V + 13] / 50)$$

$$\beta_p = 0.0065 / (1 + \exp (-[V + 15] / 28))$$

Constants

$$C_m = 1 \mu\text{F}/\text{cm}^2, V_{\text{Ca}} = 140 \text{ mV}, V_{\text{GABA}} = -75 \text{ mV}, \\ V_{\text{Glu}} = 0 \text{ mV}$$

References

- Aizenman CD, Linden DJ (1999) Regulation of the rebound depolarization and spontaneous firing patterns of deep nuclear neurons in slices of rat cerebellum. *J Neurophysiol* 82(4):1697–1709
- Aksenov DP, Serdyukova NA, Bloedel JR, Bracha V (2005) Glutamate neurotransmission in the cerebellar interposed nuclei: involvement in classically conditioned eyeblinks and neuronal activity. *J Neurophysiol* 93(1):44–52. doi:10.1152/jn.00586.2004
- Albus J (1971) Theory of cerebellar function. *Math Biosci* 10(1/2):25–61
- Allum JH, Mauritz KH (1984) Compensation for intrinsic muscle stiffness by short-latency reflexes in human triceps surae muscles. *J Neurophysiol* 52(5):797–818
- Alvarez R, Boahen K (2011) Inferior olive mirrors joint dynamics to implement an inverse controller. *Biol Cybernet* (under review)
- Alvina K, Walter JT, Kohn A, Ellis-Davies G, Khodakhah K (2008) Questioning the role of rebound firing in the cerebellum. *Nat Neurosci* 11(11):1256–1258. doi:10.1038/nn.2195
- Apps R, Garwicz M (2005) Anatomical and physiological foundations of cerebellar information processing. *Nat Rev Neurosci* 6(4):297–311. doi:10.1038/nrn1646
- Baumel Y, Jacobson GA, Cohen D (2009) Implications of functional anatomy on information processing in the deep cerebellar nuclei. *Front Cell Neurosci* 3:14 doi:10.3389/neuro.03.014.2009
- Bennett DJ (1994) Stretch reflex responses in the human elbow joint during a voluntary movement. *J Physiol* 474(2):339–351
- Berthier NE, Moore JW (1986) Cerebellar Purkinje cell activity related to the classically conditioned nictitating membrane response. *Exp Brain Res* 63(2):341–350
- Berthier NE, Singh SP, Barto AG, Houk JC (1993) Distributed representation of limb motor programs in arrays of adjustable pattern generators. *J Cognit Neurosc* 5(1):56–78. doi:10.1162/jocn.1993.5.1.56
- Chan-Palay V (1973) On the identification of the afferent axon terminals in the nucleus lateralis of the cerebellum. An electron microscope study. *Z Anat Entwicklungsgesch* 142(2):149–186
- Chorev E, Manor Y, Yarom Y (2006) Density is destiny—on [corrected] the relation between quantity of T-type Ca^{2+} channels and neuronal electrical behavior. *CNS Neurol Disord Drug Targets* 5(6):655–662
- Chun SW, Choi JH, Kim MS, Park BR (2003) Characterization of spontaneous synaptic transmission in rat medial vestibular nucleus. *Neuroreport* 14(11):1485–1488. doi:10.1097/01.wnr.0000079893.11980.a4
- De Schutter E, Steuber V (2009) Patterns and pauses in Purkinje cell simple spike trains: experiments, modeling and theory. *Neuroscience* 162(3):816–826. doi:10.1016/j.neuroscience.2009.02.040
- Fortier PA, Kalaska JF, Smith AM (1989) Cerebellar neuronal activity related to whole-arm reaching movements in the monkey. *J Neurophysiol* 62(1):198–211
- Fu QG, Flament D, Coltz JD, Ebner TJ (1997) Relationship of cerebellar Purkinje cell simple spike discharge to movement kinematics in the monkey. *J Neurophysiol* 78(1):478–491
- Fujita M (1982) Adaptive filter model of the cerebellum. *Biol Cybern* 45(3):195–206
- Gauck V, Jaeger D (2000) The control of rate and timing of spikes in the deep cerebellar nuclei by inhibition. *J Neurosci* 20(8):3006–3016
- Ghez C, Fahn S (1985) The cerebellum. In: Kandel E, Schwartz J, Jessell T (eds) *Principles of neural science*, 2nd edn. Elsevier, New York
- Hille B (2001) *Ion channels of excitable membranes*, 3rd edn. Sinauer, Sunderland
- Jahnsen H (1986) Electrophysiological characteristics of neurones in the guinea-pig deep cerebellar nuclei in vitro. *J Physiol* 372:129–147
- Kawato M, Gomi H (1992) A computational model of four regions of the cerebellum based on feedback-error learning. *Biol Cybern* 68(2):95–103
- Kistler WM, De Zeeuw CI (2003) Time windows and reverberating loops: a reverse-engineering approach to cerebellar function. *Cerebellum* 2(1):44–54. doi:10.1080/14734220309426
- Kistler WM, van Hemmen JL, De Zeeuw CI (2000) Time window control: a model for cerebellar function based on synchronization, reverberation, and time slicing. *Prog Brain Res* 124:275–297. doi:10.1016/S0079-6123(00)24023-5
- Llinas R, Muhlethaler M (1988) Electrophysiology of guinea-pig cerebellar nuclear cells in the in vitro brain stem-cerebellar preparation. *J Physiol* 404:241–258
- Llinas R, Walton K, Lang E (2004) *Cerebellum*. In: Sheperd G (ed) *The synaptic Organization of the Brain*. Oxford University Press, New York
- Mainen ZF, Sejnowski TJ (1996) Influence of dendritic structure on firing pattern in model neocortical neurons. *Nature* 382(6589):363–366. doi:10.1038/382363a0
- Manor Y, Rinzel J, Segev I, Yarom Y (1997) Low-amplitude oscillations in the inferior olive: a model based on electrical coupling of neurons with heterogeneous channel densities. *J Neurophysiol* 77(5):2736–2752
- Marr D (1969) A theory of cerebellar cortex. *J Physiol* 202(2):437–470
- Mathy A, Ho SS, Davie JT, Duguid IC, Clark BA, Hausser M (2009) Encoding of oscillations by axonal bursts in inferior olive neurons. *Neuron* 62(3):388–399. doi:10.1016/j.neuron.2009.03.023
- Monsivais P, Clark BA, Roth A, Hausser M (2005) Determinants of action potential propagation in cerebellar Purkinje cell axons.

- J Neurosci 25(2):464–472. doi:[10.1523/JNEUROSCI.3871-04.2005](https://doi.org/10.1523/JNEUROSCI.3871-04.2005)
- Raman IM, Gustafson AE, Padgett D (2000) Ionic currents and spontaneous firing in neurons isolated from the cerebellar nuclei. J Neurosci 20(24):9004–9016
- Rowland NC, Jaeger D (2008) Responses to tactile stimulation in deep cerebellar nucleus neurons result from recurrent activation in multiple pathways. J Neurophysiol 99(2):704–717. doi:[10.1152/jn.01100.2007](https://doi.org/10.1152/jn.01100.2007)
- Wetmore DZ, Mukamel EA, Schnitzer MJ (2008) Lock-and-Key mechanisms of cerebellar memory recall based on rebound currents. J Neurophysiol 100(4):2328–2347. doi:[10.1152/jn.00344.2007](https://doi.org/10.1152/jn.00344.2007)